

Investigation of the ageing conditions of PEEK powder for the selective laser sintering process

Yuqing Guo, Hu Chen, Sukun Tian, Yongxiang Xu, Kenan Ma, Shuai Ma, Xiang Wang, Yicha Zhang & Yuchun Sun

To cite this article: Yuqing Guo, Hu Chen, Sukun Tian, Yongxiang Xu, Kenan Ma, Shuai Ma, Xiang Wang, Yicha Zhang & Yuchun Sun (2023) Investigation of the ageing conditions of PEEK powder for the selective laser sintering process, *Virtual and Physical Prototyping*, 18:1, e2273298, DOI: [10.1080/17452759.2023.2273298](https://doi.org/10.1080/17452759.2023.2273298)

To link to this article: <https://doi.org/10.1080/17452759.2023.2273298>



© 2023 The Author(s). Published by Informa UK Limited, trading as Taylor & Francis Group



[View supplementary material](#)



Published online: 31 Oct 2023.



[Submit your article to this journal](#)



[View related articles](#)



[View Crossmark data](#)

Investigation of the ageing conditions of PEEK powder for the selective laser sintering process

Yuqing Guo ^{a*}, Hu Chen ^{a*}, Sukun Tian ^a, Yongxiang Xu ^b, Kenan Ma ^a, Shuai Ma ^c, Xiang Wang ^a, Yicha Zhang ^d and Yuchun Sun ^a

^aCenter of Digital Dentistry, Faculty of Prosthodontics, Peking University School and Hospital of Stomatology & National Center for Stomatology & National Clinical Research Center for Oral Diseases & National Engineering Research Center of Oral Biomaterials and Digital Medical Devices & NHC Key Laboratory of Digital Stomatology & Beijing Key Laboratory of Digital Stomatology & Key Laboratory of Digital Stomatology, Chinese Academy of Medical Sciences & NMPA Key Laboratory for Dental Materials, Beijing, People's Republic of China;

^bDepartment of Dental Materials, Peking University School and Hospital of Stomatology & National Engineering Laboratory for Digital and Material Technology of Stomatology, National Clinical Research Center for Oral Diseases, Beijing Key Laboratory of Digital Stomatology, National Medical Products Administration Key Laboratory for Dental Materials, Research Center of Engineering and Technology for Digital Dentistry, Ministry of Health, Beijing, People's Republic of China; ^cSchool of Medicine, Liaocheng University, Liaocheng, People's Republic of China; ^dMechanical Engineering and Design Department, Université de Bourgogne Franche-Comté, Université de Technologie de Belfort-Montbéliard Belfort Cedex, France

ABSTRACT

Ageing mechanism of PEEK powders at optimal powder bed temperature (T_b) and factors affecting their reusability remain unclear. This study investigated effects of gas type (air, nitrogen, and argon) and holding time (0–8 h) on physico-chemical properties of PEEK powders at optimal T_b . The hardness of sintered single-layers was measured to evaluate the quality of the parts. Results revealed that the flowability, morphology, and crystallinity of PEEK powders changed with holding time in different gases. Further, the ageing mechanism involved chain crosslinking within molecular chains in all gases but chain breakage in air. Further, laser power required for SLS decreased with the increase in holding time. However, the hardness of single-layers was stable for powders aged in argon for up to 8 h, but decreased by 7% for powders aged in nitrogen for 4 h. Severe degradation and blackening were observed for single-layers sintered in air using both virgin and aged powders.

ARTICLE HISTORY

Received 12 July 2023
Accepted 6 September 2023

KEYWORDS

Polyetheretherketone (PEEK); powder ageing; reusability; selective laser sintering; mechanical property

1. Introduction

Selective laser sintering (SLS) is an important branch of laser powder bed fusion, which uses powders to create solid parts layer by layer through laser scanning of the building platform [1–5]. It was invented in the 1980s and led to the formation of DTM Corp. [6]. After being acquired by 3D Systems, Inc., the term 'Laser Sintering' became synonymous with SLS in the industry [7–10]. SLS has the advantage of printing prototypes with multi-functional, complex, and customised freeform structures without support structures. The semi-crystalline thermoplastic polyamide (PA) is the most common commercial material for SLS [11–13]. However, PA has a low melting

temperature (T_m) and glass transition temperature (T_g), which restrict its application at high-temperatures [14]. Since the appearance of the first commercial high-temperature SLS machine, the EOSINT P800 printer (EOS GmbH, Krailling, Germany), the SLS of high- T_m polymers, especially polyetherketone (PEK) and polyetheretherketone (PEEK), has been explored [15–19].

Beard et al. were the first to study the high-temperature laser sintering of PEK (HP3, EOS) using a standard high-temperature SLS machine [19]. They achieved fully dense PEK samples with fine surface by setting the processing temperature to 366 °C, and the samples had consistent thermal and mechanical properties

CONTACT Yuchun Sun  kqsyrc@bjmu.edu.cn Xiang Wang  xiangwang@hsc.pku.edu.cn  Center of Digital Dentistry, Faculty of Prosthodontics, Peking University School and Hospital of Stomatology & National Center for Stomatology & National Clinical Research Center for Oral Diseases & National Engineering Research Center of Oral Biomaterials and Digital Medical Devices & NHC Key Laboratory of Digital Stomatology & Beijing Key Laboratory of Digital Stomatology & Key Laboratory of Digital Stomatology, Chinese Academy of Medical Sciences & NMPA Key Laboratory for Dental Materials, Beijing, 100081, People's Republic of China; Yicha Zhang  yicha.zhang@utbm.fr  Mechanical Engineering and Design Department, Université de Bourgogne Franche-Comté, Université de Technologie de Belfort-Montbéliard, ICB UMR CNRS 6303, 90010 Belfort Cedex, France

*These authors contributed equally to this work.

 Supplemental data for this article can be accessed online at <https://doi.org/10.1080/17452759.2023.2273298>.

© 2023 The Author(s). Published by Informa UK Limited, trading as Taylor & Francis Group

This is an Open Access article distributed under the terms of the Creative Commons Attribution-NonCommercial License (<http://creativecommons.org/licenses/by-nc/4.0/>), which permits unrestricted non-commercial use, distribution, and reproduction in any medium, provided the original work is properly cited. The terms on which this article has been published allow the posting of the Accepted Manuscript in a repository by the author(s) or with their consent.

within and between batches. However, they also observed severe degradation as a result of crosslinking in the PEK powders that were exposed to such high-temperature, which EOS GmbH advised not to reuse [18]. Notably, the degraded PEK powders had increased melting temperature and crystallinity, which required higher than normal laser power to scan the build platform. When the laser power was increased by 10%, the blended powders with aged and virgin PEK (30 wt.%/70 wt.% used/virgin) showed a 16% reduction in tensile strength and elongation at break [18].

PEEK, which has a T_m of 343 °C (about 30 °C lower than PEK), is more suitable for SLS because it reduces the difficulty in temperature control and the subsequent degradation effects [15]. In addition, PEEK has high thermal resistance, excellent mechanical properties, and biocompatibility, which make it attractive for SLS applications in the aerospace and automobile industries, as well as clinical medicine [1, 10, 20]. PEEK samples (PEEK 450PF, Victrex) have been successfully fabricated using the same standard high-temperature SLS machine [16]. The PEEK 450PF powders were thermally treated before printing to improve the particle flow and shape, and then sintered with an optimised process. The tensile strength of the PEEK specimen was 63 MPa, about 20 MPa lower than that of PEK. Various additives such as carbon fibre, graphite platelets, and nanoparticles have been used to improve the properties of PEEK in SLS [15, 21, 22]. For example, adding 10 wt.% of carbon fibre (CF) enhances the mechanical properties of PEEK composites, and the tensile strength of the sintered CF/PEEK samples reached 109 ± 1 MPa, which meets the requirements of the aerospace industry [21].

One of the drawbacks of SLS technology is the low powder utilisation rate, which means that only a small fraction of polymer powders is converted into the final solid parts, and the rest is discarded [23]. There are two types of raw powder waste: one is the leftover unsintered powders on the build platform, and the other is the surplus feeding powder that falls into the recovery tank [24]. Further, the SLS of PEEK requires high-temperatures; for example, the part bed temperature (T_b) is usually set just below the T_m of the polymer throughout the process [23, 25]. The theoretical T_b is recommended to be set at the minimum point of the first derivative of the DCS curve in the heated segment [26, 27]. Dynamic non-isothermal crystallisation and quasistatic isothermal crystallisation indicated that the practical T_b of PEEK powder is around 332 °C [26, 28]. By setting T_b at such high-temperatures, PEEK composites can be successfully sintered into 3D shapes [20, 21]. Therefore, the unsintered PEEK powders on the building platform, which act as a support structure for the parts, undergo severe

thermal effects under such high-temperature exposure for several hours until the printing is finished [29, 30]. Moreover, because of its unique characteristics and high performance, the commercially available PEEK powder is very expensive. Therefore, it is crucial to understand the thermal ageing mechanism and potential reuse of PEEK powder.

The reuse of PEEK has been evaluated in a self-developed powder bed fusion system, where the strength of sintered samples using aged powders increased in the first cycle but then decreased [31]. Further, large warping deformation was observed after the fourth cycle, indicating unsuitable for SLS any more. The addition of carbon fibre effectively reduced this deformation, yielding a higher strength in the second cycle. However, the processing time and atmosphere used in each printing cycle were not reported, and the total holding time of the un-sintered powders in each print cycle is unknown. Another study found that the tensile strength of high-temperature SLS polymers reached the highest when sintered with a holding time for 6.25 h, but did not investigate the physico-chemical changes of the un-sintered powders under such conditions yet [27].

For simulating T_b of PEEK, Pate et al. investigated the spectroscopic, morphological, and rheological changes of PEEK powders after thermal treatment at 330 and 340 °C for different periods [23]. The aged powders had unchanged particle size and shape, but improved flowability. However, the melting point and decomposition rates of the PEEK powder were increased after ageing over 6 h, indicating their poor recyclability. Protective gas was suggested to be used in SLS to prevent thermo-oxidative degradation, but previous study was only carried out in air, which undermined the recyclability of PEEK [23]. A similar study to evaluate the ageing mechanism of PEEK powders was carried out by layer-wise infrared radiation at 250–300 °C for 5 h [32]. The results showed that powder morphology became more regular and uniform after thermal treatment, and ageing was caused by the formation of a biphenyl structure and the reduction in crystallinity. However, the ageing gas condition was not presented, and the temperature parameters were much lower than those in SLS of PEEK. These studies have helped us to understand the changes in the physico-chemical properties of thermally treated PEEK powders, but the experimental conditions (e.g. temperature, gas condition, and holding time) did not match those of PEEK in practical SLS; specifically, PEEK powders are sintered at about 330 °C under the protection of inert gas [1, 33].

Nitrogen and argon are recommended as the protective gas in the high-temperature SLS of PEEK, but the changes in un-sintered PEEK powders in different

sintering gases have not been systematically studied [1, 33]. Considering that the PEEK powders were severely degraded after thermal ageing for 6 h and the mechanical strength reached the maximum on holding for 6.25 h in previous studies, ageing times from 0 to 8 h at the optimal T_b of 330 °C in different gas atmosphere were used in this study [23, 27]. To verify the importance of protective gases in the high-temperature SLS of PEEK, the physico-chemical behaviours of powders aged in air were also investigated.

In this study, we systematically evaluated the factors of ageing (e.g. gas type and holding time) and their influence on the reusability of PEEK powders, and propose a reference for reusing aged powders. The particle size distributions (PSDs), bulk density, flowability, morphology, melting/crystallisation properties, thermal stability, and ageing mechanism of virgin and thermally aged PEEK powders were thoroughly investigated. Then, single-layer films of virgin and 100 wt.% aged PEEK powders aged under different conditions were sintered using optimised parameters in the corresponding atmosphere. The results suggest that both argon and nitrogen can effectively prevent degradation in the high-temperature SLS of virgin and aged PEEK, whereas serious degradation was observed in air. Only a 2% reduction in hardness was found in single-layer parts sintered by powders aged in argon for 8 h, but a 7% reduction was found even for the 4 h by powders aged in nitrogen. Besides, the laser power should be gradually reduced when reusing powders either ageing in nitrogen or argon.

2. Materials and methods

2.1. Materials and thermal ageing protocols

Virgin PEEK powder (PEEK 330PF, JiLin Joinature Polymer Co., Ltd, China) was vacuum dried before the SLS process to improve its flowability. The average particle size (D_{50}) was 50 μm , and the T_g of the powder was 143 °C. The onset of the melting temperature ($T_{m(\text{onset})}$) of virgin PEEK powders was characterised at 332 °C by DSC analysis (Figure S1, supplementary material).

A simplified building chamber was used to simulate the SLS ageing process, and the scheme for the experimental setup is shown in Figure 1a. Thermal baffles were used to construct the main structure of the heating chamber, integrated with four 500 W infrared lamp tubes and two ventilation ports, which could withstand temperatures up to 1000 °C. The powder samples were spread in a crucible, placed in the chamber and purged with dry gas flow of air (A), nitrogen (N), or argon (Ar) at a rate of 5 L/min. The temperature was controlled by a thermocouple inside the chamber. To avoid

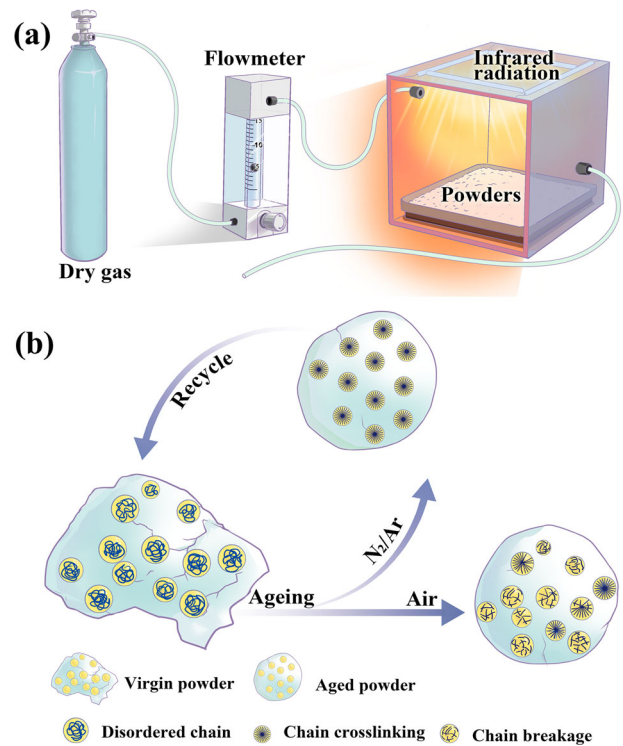


Figure 1. Scheme of (a) experimental setup of the simulating ageing condition in SLS system and (b) observed ageing mechanism.

powder melting and simulate the temperature in SLS, the powder samples were heated to 330 °C and maintained at the isothermal stage from 2~8 h. The samples were denoted x-2, x-4, and x-8, respectively, where x = A, N, or Ar. Finally, the powder samples were slowly cooled to room temperature under continuous gas flow and then stored in a dry, airtight environment.

2.2. Fabrication of virgin and aged PEEK samples by SLS

Virgin and thermally aged PEEK powders were sintered using a self-developed SLS system with a 10 W continuous wave (CW) glass fibre laser ($\lambda = 1.06 \mu\text{m}$). Before printing, dry gas was continuously injected until the chamber was filled with the corresponding gas; then, the powder samples were spread on the platform and heated to 330 °C. The process parameters are shown in Table S1, supplementary material. After sintering, the samples were kept in the chamber until cooling to room temperature and, then, removed from the residual powder.

2.3. Tests and characterisation

The particle size distributions (PSDs) of the virgin and thermally aged PEEK powders were measured using a laser particle size analyser (Malvern Mastersizer 2000,

UK) after ultrasonically dispersing the powders in ethanol. The angle of repose (AOR) was measured using a powder flowability tester (Yishite, ST-16913, China) following the ASTM C1444 standard [34], and the bulk density was tested following the GB/T 16913-2008 procedure (Yishite, ST-1003, China) [35]. The morphologies of PEEK particles and fabricated samples were characterised by scanning electron microscopy (SEM; HITACHI-SU8020 and Hitachi Regulus 8100, Japan). All samples were sputter-coated with gold before SEM measurement.

The thermal behaviours of the virgin and thermally aged PEEK powders were determined by differential scanning calorimetry (DSC; DSC250, TA instruments, US) according to the following programme under nitrogen protection at a gas flow rate of 50 mL/min (GB/T 19466-20004 [36]): 25–400 °C at a heating rate of 10 °C/min (isothermal for 5 min), 400–50 °C at a cooling rate of 10 °C/min (isothermal for 5 min); then, the temperature was raised up to 400 °C at a heating rate of 10 °C/min. About 10 mg of each specimen was heated in an aluminium crucible and each analysis was performed three times. The degree of crystallinity from DSC ($X_{c(DSC)}$) was examined and calculated using Equation (1):

$$X_{c(DSC)} = (\Delta H_m / \Delta H_{m(100\%)}) * 100\% \quad (1)$$

Here, ΔH_m is the melting endotherm, and $\Delta H_{m(100\%)}$ is the melting enthalpy of fully crystalline PEEK (130 J/g) [37].

Thermogravimetric analysis (TGA; TG-DSC 3+, Mettler) was carried out to evaluate the degradation temperature of the virgin and thermally aged PEEK powders. Samples were heated from room temperature to 900 °C with a heating rate of 10 °C/min under a nitrogen atmosphere.

X-ray diffraction (XRD) patterns of the virgin and thermally aged PEEK powders were obtained by an X-ray diffractometer (D8 Advance, Bruker, Germany) using Cu- K_α X-rays ($\lambda = 1.5406 \text{ \AA}$) generated at 40 kV and 40 mA running from $2\theta = 4$ to 65° at a scanning speed of $3^\circ/\text{min}$. The crystallite sizes and interplanar distance were calculated according to the Scherrer equation (Equation (2)) and Bragg's Law (Equation (3)), respectively [2, 23, 38]. The degree of crystallinity from XRD ($X_{c(XRD)}$) was calculated using Equation (4):

$$L = K\lambda / (FWHM(2\theta)\cos\theta) \quad (2)$$

$$d = \lambda / 2\sin\theta \quad (3)$$

$$X_{c(XRD)} = \Sigma S_C / (\Sigma S_A + \Sigma S_C) * 100\% \quad (4)$$

Here, L is the apparent crystal thickness of the crystallite perpendicular to one specific (hkl) plane [2, 28, 38], and d is the interplanar distance, K is the Scherrer

constant ($K = 0.89$) [39], and λ refers to the X-ray wavelength. FWHM is the full width at half-maximum width of the diffraction peak in radians, θ is the Bragg angle in radians, S_A is the integration of the amorphous peak area, and S_C is the integration of the crystalline peak area.

The Fourier transform infrared (FTIR) spectra of the virgin and thermally aged PEEK powders were obtained by using a spectrometer (Nicolet iS10, Thermo Fisher Scientific Inc., US) between 4000 and 400 cm^{-1} with a step size of 0.48 cm^{-1} . The Vickers hardness of the fabricated films was measured on planar sintered areas by an ARTRAY digital Vickers microhardness tester at a load of 0.98 N for 15 s at room temperature. The average of nine readings was taken for each group. The experimental workflow is shown in Figure 2.

2.4. Statistical analyses

Statistical analyses were performed with IBM SPSS Statistics 19.0 (Armonk, NY, USA) using one-way ANOVA and Tukey's honest significant difference (HSD) test at a significance level of 0.05. The results are expressed as the mean value \pm standard deviation.

3. Results and discussion

3.1. Improved powder spreading property for aged PEEK powders

PEEK powders showed diverse colours after thermal ageing under different conditions (Figure 3). Limited changes were observed in nitrogen and argon even after thermal ageing for 8 h, but the powders gradually faded to yellow when thermally aged in air. Powder characterisation, including PSDs, flowability, and bulk density, were studied in detail to evaluate the influence of the ageing conditions on the spreading properties of the PEEK powders.

The PSDs of the virgin and thermally aged PEEK powders are shown in Figure 4. The particle size of both virgin and thermally aged PEEK powders showed a bimodal distribution (Figure 4a–c). In particular, the proportion of particles at the lower peak position were gradually reduced with the increase in holding time when thermally aged in air, whereas those at the higher peak position were gradually concentrated (Figure 4a). Additionally, the 100% cumulative percentage of aged PEEK powders showed narrower PSDs, where both the proportions of small and large particles were slightly decreased in the aged powders (Figure 4d, Table S2, supplementary material). This phenomenon was also detected in PEEK powders thermally aged in

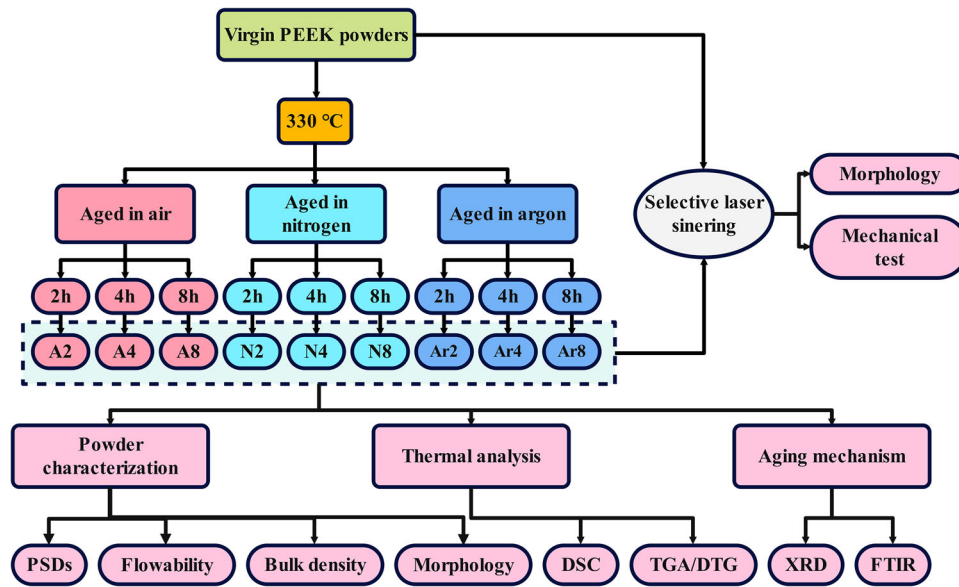


Figure 2. Experimental workflow.

nitrogen and argon (Figure 4e, f). The decrease in the proportion of small particle sizes was caused by fusion between small particles, whereas the decrease in large particle sizes was caused by the melting and shrinking of irregular edges. Narrower PSDs are expected to enhance the powder flowability during powder spreading in SLS, thus indicating the recyclability of thermally aged PEEK powders [10].

The AOR is also an important parameter for powders in SLS and used to evaluate the flowability of powder. Specifically, a small angle ($<40^\circ$) indicates fine flowability [23]. As shown in Table 1, the virgin PEEK powder

presented a high AOR value larger than 43° , indicating low ability to spread uniformly in the build platform during powder bed fusion. Further, the AOR value significantly decreased after ageing at 330°C in air, nitrogen, and argon. The value was smaller than 40° and further slightly decreased with holding time. The changes in these factors suggest that the thermally aged PEEK powders have the potential for reuse and recycling.

Bulk density is another important evaluation parameter for powders in SLS, representing the density of uncompressed powder per unit volume. A high bulk

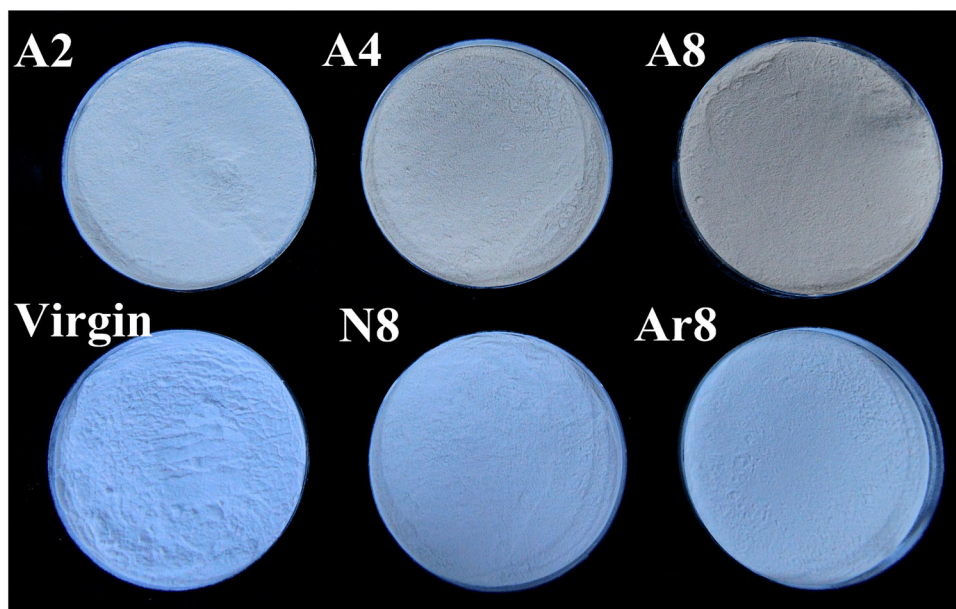


Figure 3. Digital photos of virgin and thermally aged PEEK powders.

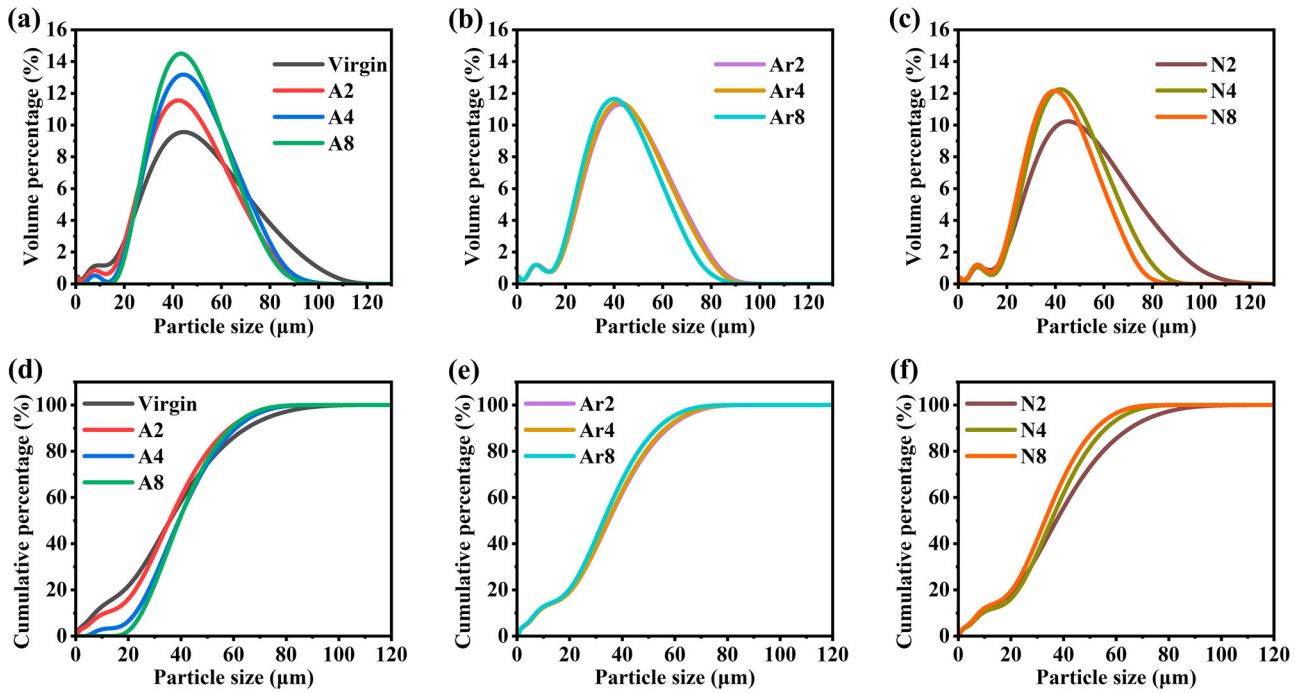


Figure 4. PSDs of virgin and thermally aged PEEK powders under different ageing conditions: (a–c) volume percentage and (d–f) cumulative percentage.

density is necessary for the creation of defect-free samples [26, 29]. The bulk densities of virgin and thermally aged PEEK powders under different ageing conditions are presented in Table 1. The average bulk density of virgin PEEK was found to be near 0.47 g/cm^3 , and it was slightly increased after thermal ageing, where all aged groups showed bulk densities higher than 0.51 g/cm^3 .

The powder spreading property showed the same trend with respect to holding time in all three gases. Although the powder spreading was gradually improved with time, there were no statistically significant differences between holding times or ageing gas conditions, and no evident variations within 2 h were observed. On the basis of the data analysis, the changes in PSDs, AOR and bulk density were completed within 2 h. The minimal changes in these factors suggest that the

thermally aged PEEK powders have the potential for reuse and recycling.

3.2. Morphologies of virgin and thermally aged PEEK powders

The morphological differences between the virgin and thermally aged PEEK powders were observed by SEM. The virgin PEEK powders had two typical structures: irregular and non-uniform spherical structures and flakes (Figure 5a, b). Upon further magnification, the particles had sharp edges, where microcracks were visible inside (Figure 5c). The powders became more regular and uniform after thermal ageing, without any agglomeration (Figure 5d–l). However, the particles still had spherulitized edges and corners with microcracks inside. The distance between the microcracks decreased with ageing time, and the surface became denser (Figures S2–S4, supplementary material). Moreover, small flakes adhered to the spherical structure in the aged PEEK powders (Figure 5f, i, l). These results suggested that melting and fusion occurred within and between particles. The surface of the powders seemed smoother and denser after thermal ageing in nitrogen and argon than in air (Figures S2–S4, supplementary material). In addition, there was no significant morphology difference between powders aged in nitrogen and argon.

A smooth and spherical surface helps reduce the friction between particles, increase the flowability, and

Table 1. Angle of repose and bulk density of virgin and thermally aged PEEK powders.

Atmosphere	Group	Angle of repose (°)	Bulk density (g/cm^3)
–	Virgin	43.14 ± 2.95	0.4657 ± 0.0036
Air	A2	39.67 ± 4.15	0.5145 ± 0.0094
	A4	39.19 ± 2.76	0.5248 ± 0.0033
	A8	39.12 ± 1.52	0.5149 ± 0.0045
	Nitrogen		
Nitrogen	N2	39.44 ± 1.27	0.5180 ± 0.0014
	N4	38.63 ± 1.98	0.5177 ± 0.0030
	N8	37.43 ± 2.47	0.5181 ± 0.0034
Argon	Ar2	38.36 ± 2.44	0.5174 ± 0.0071
	Ar4	38.28 ± 2.00	0.5235 ± 0.0042
	Ar8	37.17 ± 1.74	0.5224 ± 0.0037

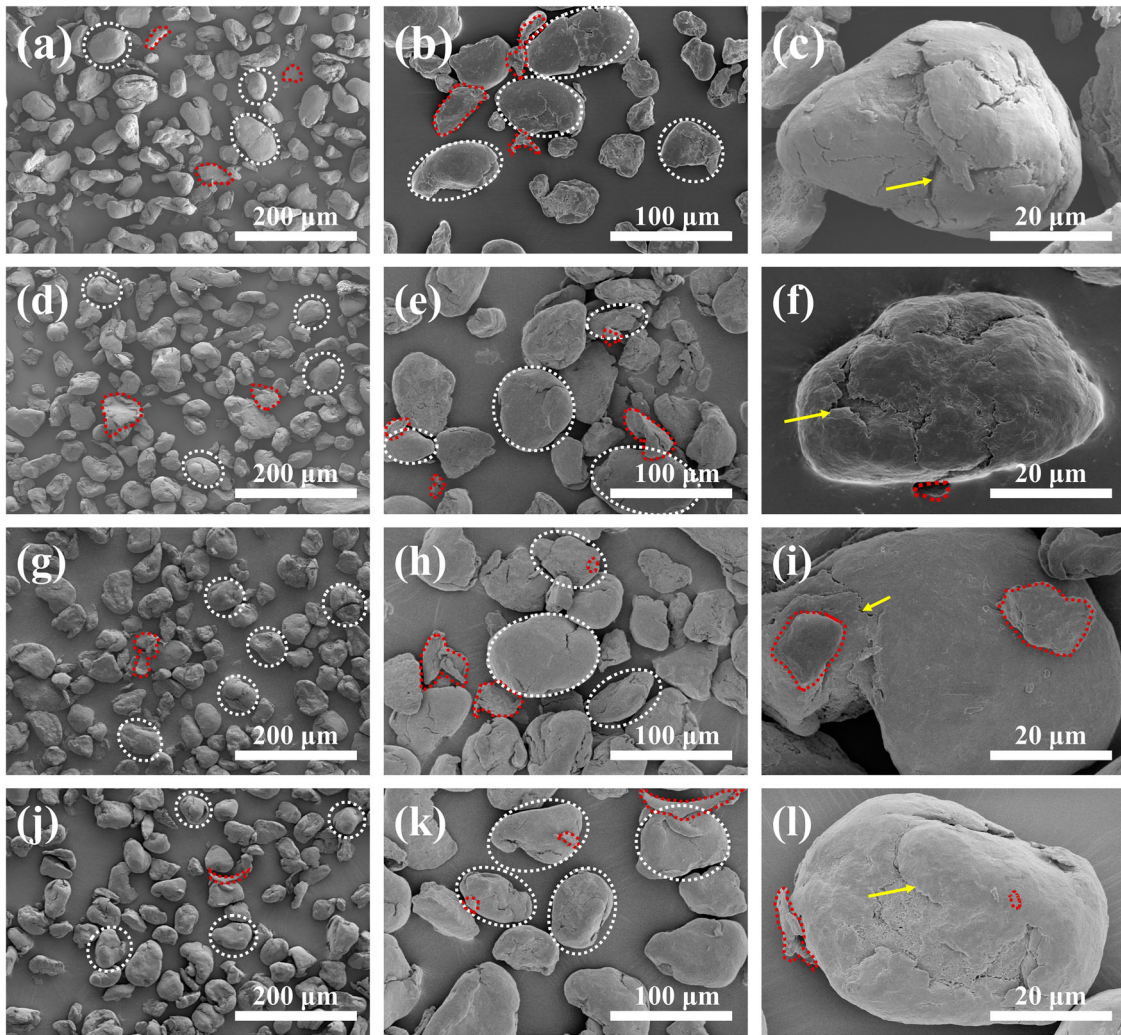


Figure 5. Morphologies of virgin (a–c), and aged PEEK powders in A8 (d–f), N8 (g–i), and Ar8 (j–l) with different magnifications. White circles denote spherical structures, red denotes flakes, and arrows denote microcracks.

enhance the processability during powder spreading [37]. However, the attachment of some small flakes might increase the friction between particles and reduce flowability instead. Although the AOR values were reduced in aged PEEK powders, they did not explain

some conflicting results revealed by SEM. Particularly, these results suggest that the flowability is affected by the competition and interaction between the spherical and flaky structures, and more methods should be proposed to measure powder spreading in the future.

Table 2. Thermal information from DSC data of virgin and thermally aged powders.

Group	$T_{c(\text{peak})}$ (°C)	$T_{c(\text{onset})}$ (°C)	$T_{m(\text{onset})}$ (°C)	$T_{m(\text{peak})}$ (°C)	ΔH_m (J/g)	$X_{c(\text{DSC})}$ (%)	ΔH_c (J/g)
Virgin	293.87 ± 2.40	303.57 ± 0.71	332.07 ± 1.44	342.70 ± 0.64	31.44 ± 2.44	24.18 ± 1.87	43.07 ± 1.71
A2	304.50 ± 1.35	311.83 ± 1.89	333.32 ± 0.87	343.70 ± 0.12	30.81 ± 0.40	23.70 ± 0.30	43.74 ± 1.20
A4	306.25 ± 1.64	313.54 ± 2.16	333.09 ± 0.86	344.09 ± 0.28	30.09 ± 1.72	23.15 ± 1.32	45.09 ± 1.38
A8	306.59 ± 0.96	313.89 ± 1.51	332.64 ± 0.99	344.44 ± 0.48	29.84 ± 2.00	22.95 ± 1.54	47.23 ± 2.43
N2	298.15 ± 0.54	305.91 ± 0.36	332.64 ± 0.06	342.78 ± 0.19	30.67 ± 2.02	23.59 ± 1.56	45.22 ± 0.25
N4	298.37 ± 0.44	306.59 ± 0.75	332.63 ± 0.37	343.09 ± 0.38	30.57 ± 2.15	23.51 ± 1.65	45.70 ± 1.91
N8	303.86 ± 0.73	311.09 ± 0.97	333.32 ± 0.78	343.97 ± 0.48	29.88 ± 2.24	22.98 ± 1.72	46.84 ± 3.10
Ar2	300.26 ± 0.23	307.62 ± 0.84	332.64 ± 0.19	343.50 ± 0.04	30.97 ± 2.14	23.82 ± 1.65	44.46 ± 1.16
Ar4	301.72 ± 0.83	308.36 ± 1.12	332.64 ± 0.47	343.71 ± 0.10	29.25 ± 2.06	22.50 ± 1.58	45.01 ± 2.07
Ar8	303.81 ± 1.57	310.75 ± 1.93	332.29 ± 0.53	344.28 ± 0.47	28.56 ± 1.67	21.97 ± 1.29	45.92 ± 0.92

* $T_{c(\text{onset})}$ and $T_{c(\text{peak})}$ are the onset temperature and peak temperature of crystallisation, respectively. $T_{m(\text{onset})}$ and $T_{m(\text{peak})}$ are the onset temperature and peak temperature of melting, respectively. ΔH_m and ΔH_c are the melting enthalpy and crystallisation enthalpy, respectively. $X_{c(\text{DSC})}$ is the degree of crystallisation from DSC.

3.3. Thermal properties and sintering window analyses by DSC

The samples were analyzed using standardized heating-cooling cycles as described in the experimental section. Table 2 shows the results from the DSC measurements of virgin and aged PEEK powders with crystallinity, enthalpy, onset temperature, and peak temperature during the melting and crystallisation processes.

The DSC curves of virgin and thermally aged PEEK powders under different ageing conditions are shown in Figure 6. The $T_{c(\text{peak})}$ and $T_{c(\text{onset})}$ of the virgin PEEK powders were 293.87 ± 2.40 and 303.57 ± 0.71 °C, respectively. As the holding time increased, the crystallisation temperatures (T_c) shifted slightly to higher temperatures ($T_{c(\text{air})} > T_{c(\text{nitrogen})} \approx T_{c(\text{argon})}$) (Figure 6a). Crosslinking occurred inside the molecular chains with the extending of holding time, resulting in molecular weight and T_c increasing. Although polymer chain breakage occurs within samples aged in an oxygen-containing atmosphere, resulting in reduced molecular weight and T_c [32, 40, 41], oxygen also found facilitating the crosslinking within a few hours [42, 43]. Therefore, higher T_c in powders aged in air than those of in powders aged in nitrogen and argon can be attributed to the dynamic's competition between crosslinking and breakage.

The aged PEEK powders showed increased changing in the enthalpy of crystallisation (ΔH_c), and this further increased with the increase in holding time in all experimental atmospheres (Table 2). There was no statistically significant difference in crystallisation between the powders aged in nitrogen and argon when held for the same time. Further, a secondary melting endotherm was not found in aged powders, but a slight increase in the melting peak was observed along with a decrease in melting enthalpy and crystallinity (Figure 6b, Table 2). PEEK is a semi-crystalline polymer, where the chains between the crystalline

and amorphous regions are braked [44]. Chain scission and crosslinking could be observed after thermal ageing at high-temperatures, and the amorphous regions tended to form ordered, preferential crystals because of crystalline reorganisation, which reduces the molecular mobility, inhibits annealing, and further causes decreased crystallinity [23, 24]. This suggests that the slight increase in the melting temperature is due to crystalline reorganisation rather than an increase in crystallinity.

By describing crystallisation speed, the sintering window (SW) can be used to determine the eventual nucleation behaviour of the particles within the matrix [26]. The results showed that the changes in $T_{m(\text{onset})}$ after thermal ageing were negligible, whereas $T_{c(\text{onset})}$ gradually increased with the increase in holding time, causing a narrower SW. A narrower SW indicates a higher nucleation value and faster crystallisation speed, implying that a smaller supercooling region is required to activate crystallisation as the cooling rate increases [45, 46]. On the one hand, the narrower SW results in more difficulty in controlling T_b , which should be set accurately with a narrow temperature range. On the other hand, the limited changes in $T_{m(\text{onset})}$ are helpful for the temperature setting when simultaneously using virgin and reused PEEK powders. Therefore, T_b should be set close to $T_{m(\text{onset})}$ within a minimal range of fluctuations when reusing the aged PEEK powders.

3.4. Degradation analyses

The TGA and derivative thermogravimetric (DTG) curves of virgin and thermally aged PEEK powders under different ageing conditions are shown in Figure 7a and b, respectively. The corresponding data are presented in Table 3, including the 1% weight loss temperature (T_1), 5% weight loss temperature (T_5), 30% weight loss

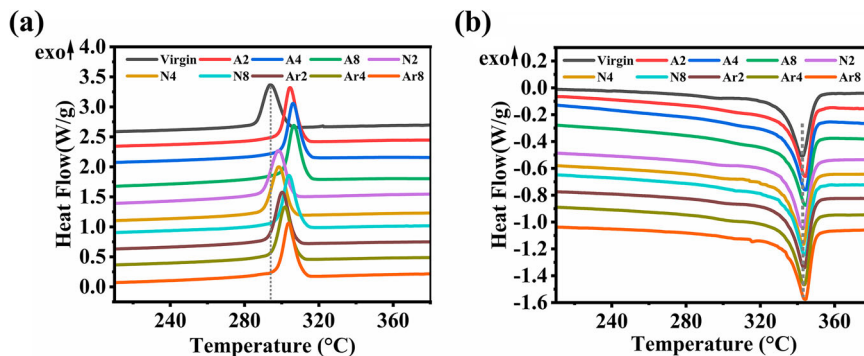


Figure 6. DSC thermograms of virgin and thermally aged PEEK powders under different ageing conditions: (a) cooling and (b) heating.

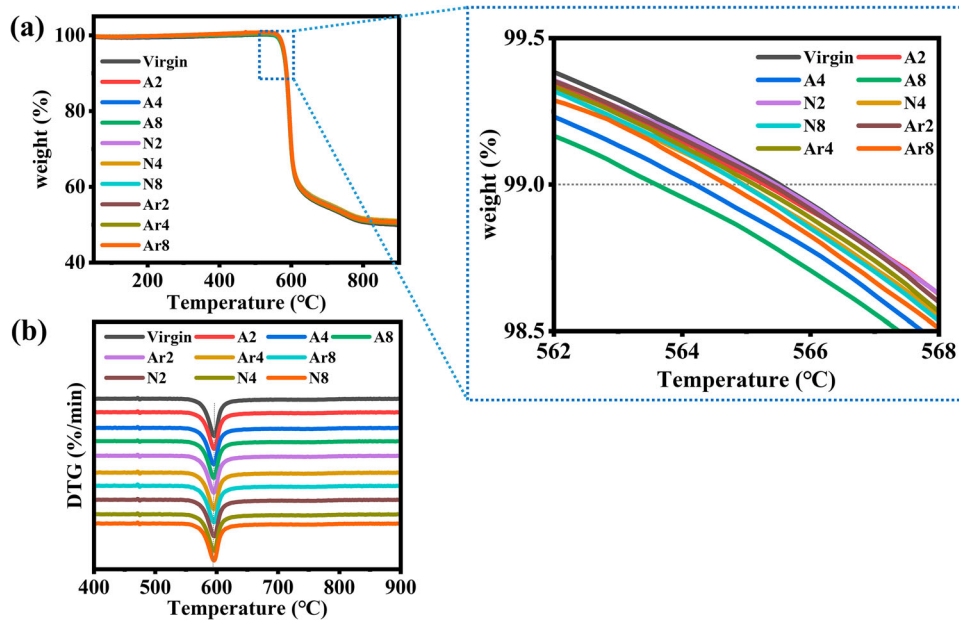


Figure 7. (a) TGA and (b) DTG curves of virgin and thermally aged PEEK powders under different ageing conditions.

temperature (T_{30}), and maximum decomposed ratio temperature (T_{max}).

Because of their high heat resistance and long molecular chains, PEEK powders have high decomposition temperatures. As shown in Table 3, the T_1 , T_5 , T_{30} and T_{max} of the virgin PEEK powders were approximately 565, 580, 600, and 596 °C, respectively. When below 565 °C, the weight loss of virgin PEEK powders was negligible, which was consistent with the DTG curve (Figure 7b). The heat resistance slightly decreased with the increase in holding time after thermal ageing in all gas conditions. However, the changes in the TGA and DTG curves between virgin and thermally aged PEEK powders were very minor and insignificant, meaning that thermal ageing at 330 °C in air, nitrogen, or argon up to 8 h had limited effects on the thermal resistance of PEEK powders in SLS.

Table 3. TGA/DTG data of virgin and thermally aged PEEK powders under different ageing conditions.

Group	T_1 (°C)	T_5 (°C)	T_{30} (°C)	T_{max} (°C)
Virgin	565.43	580.43	600.48	596.16
A2	565.28	580.23	600.48	595.96
A4	564.31	579.75	599.65	595.18
A8	563.68	579.21	599.65	595.09
N2	565.41	579.85	600.15	596.03
N4	565.01	579.71	599.93	595.41
N8	565.01	579.57	599.76	595.53
Ar2	565.34	579.65	599.67	595.29
Ar4	565.15	579.39	599.69	595.34
Ar8	564.74	579.39	599.77	595.42

* T_1 , T_5 , and T_{30} refer to the 1%, 5% and 30% weight loss temperature, respectively. T_{max} refers to the temperature relative to maximum decomposition.

3.5. Changes in crystallisation

XRD provides information about the crystalline structural changes of PEEK powders before and after thermal treatment, and the results are shown in Figure 8. The main diffraction peaks of virgin PEEK powders were observed at 2θ values of $18.74 \pm 0.03^\circ$, $20.65 \pm 0.08^\circ$, $22.68 \pm 0.02^\circ$, and $28.78 \pm 0.03^\circ$, corresponding to the α -crystal crystalline planes of (110), (111), (200), and (211), respectively [20, 30, 32, 47]. Similar diffraction peak positions were also observed in thermally aged PEEK powders, indicating that thermal ageing did not change the crystal structure of the PEEK powders [48]. XRD patterns with sharp peaks indicate high crystallinity, whereas broad peaks indicate amorphous or disordered internal structures. Sharper peaks were found in thermally aged powders under the three experimental gas types, and the intensity was slightly increased with holding time. This suggests that the arrangement of macromolecular chains in the crystal structure is gradually more ordered after thermal ageing, consistent with the slight increase in T_m detected by DSC [28, 32].

PEEK has an orthorhombic unit cell, and the unit cells in the crystalline spherulites align along the spherulite radius, whereas the polymer backbones align along the polymer c-axis parallel to the lamellar length dimension and spherulite radius [20, 49–51]. To calculate the volume of the orthorhombic unit cell, the cell parameters were obtained using the crystalline peaks from the XRD patterns and using Equations (5–7):

$$a = \lambda / \sin \theta_{200} \quad (5)$$

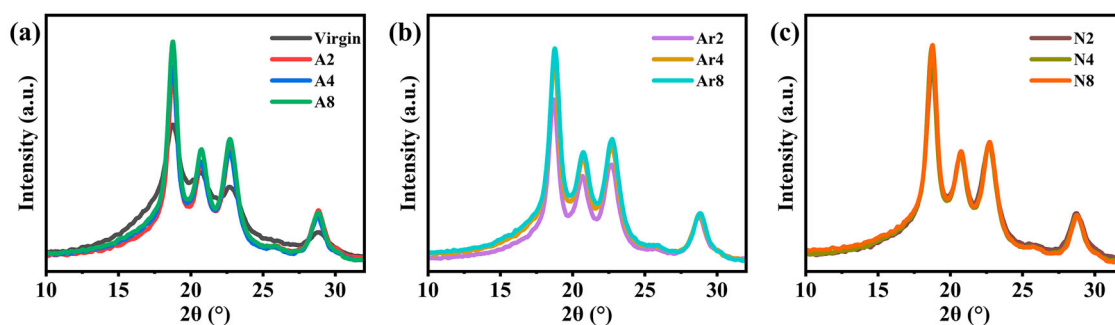


Figure 8. Diffraction patterns of virgin and thermally aged PEEK powders in (a) air, (b) argon, and (c) nitrogen. The corresponding crystallographic planes of four major crystalline peaks are marked.

$$b = (4 \sin^2 \theta_{110} / \lambda^2 - 1/a^2)^{-1/2} \quad (6)$$

$$c = (4 \sin^2 \theta_{111} / \lambda^2 - 1/a^2 - 1/b^2)^{-1/2} \quad (7)$$

Here, λ (1.5406 Å) is the X-ray wavelength and $\theta_{(hkl)}$ refers to the angular position of the (hkl) reflection [48, 52].

Table 4 lists the changes in the unit cell parameters and the calculated crystal data of virgin and thermally aged PEEK powders. The most significant changes in thermally aged PEEK powders were the reduced lattice parameter and lattice volume, indicating that macromolecular chains were packed and spaced more closely. In addition, the interplanar distance gradually decreased with increasing holding time, likely caused by shorter distances between phenylene ring subunits inside the plane [32]. Thus, as thermal ageing proceeds, the crystal structure of aged PEEK powders become more ordered with reduced lattice volume and interplanar spacing, consistent with previous studies [23, 32].

Both XRD and DSC can be effectively used to evaluate the crystallinity of PEEK samples [49]. The trend of crystallinity change in XRD analysis was similar to that in the DSC curve: the crystallinity gradually decreased with holding time when thermally aged in three gas conditions. However, $X_{c(XRD)}$ was higher than $X_{c(DSC)}$ because $X_{c(XRD)}$ considers the secondary and primary crystallites, while $X_{c(DSC)}$ only refers to the melting of the primary crystallites [49, 50].

3.6. Ageing mechanism under different gas conditions

The results from Section 3.1 to Section 3.5 indicate that the changes in thermally aged PEEK powders in the three experimental gases show the same trend over holding time. The main difference was that the SW in air was narrower than that in nitrogen and argon, whereas there was no significant difference between nitrogen and argon. To evaluate the influence of

ageing conditions on PEEK powders, FTIR analysis was used to characterise the chemical structure of virgin and thermally aged PEEK powders. Although the DSC and TGA/DTG curves indicate that little degradation occurred in all thermally aged PEEK powders, the FTIR spectra showed different behaviour (Figure 9), suggesting that multiple methods should be used to investigate the changes in the physico-chemical properties of polymers.

The chemical repeat unit of the PEEK polymer is shown in Figure 9a. The intensities of the C–H stretching vibration in benzene (3066 and 3042 cm^{-1}) gradually decreased with the increase in holding time in air, nitrogen, and argon (Figure 9b), caused by the reduced interplanar spacing and lattice volume after thermal ageing [32]. In addition, new absorption bands in the non-aromatic hydrogen carbon were found at 2916 and 2849 cm^{-1} after thermal ageing in air, and the intensities increased with the increase in holding time. This is likely due to chain scission occurring in the PEEK monomers at the applied temperature, indicating that the material was oxidized at high-temperatures and the molecular chains were partially broken [44, 53]. This verified that despite the chain breakage in PEEK powders in an oxygen-containing atmosphere, crosslinking played the dominant role in the thermally ageing, resulting in the increase of T_c observed in the DSC curve. Interestingly, peaks located at these wavenumbers were not found even after ageing for 8 h in nitrogen and argon, illustrating that the molecular chain did not break at 330 °C under nitrogen or argon protection.

The absorption bands at 1253 and 1144 cm^{-1} correspond to the stretching vibrations of $-\text{C}=\text{O}-\text{C}$, which were slightly decreased in aged PEEK powders, proving that the $-\text{C}=\text{O}-\text{C}$ bond stretching vibration was limited by the ordered crystalline structure and reduced lattice volume (Figure 9c) [32]. The C–H absorption peaks at 835 and 860 cm^{-1} correspond to the 1,4-disubstituted benzene of virgin PEEK powder. Further, new C–H wagging vibrations at 747 and 847 cm^{-1} gradually

Table 4. Crystal values of the virgin and thermally aged PEEK powders.

Group	Crystal plane	2θ (°)	FWHM (°)	$L_{(hkl)}$ (Å)	d (Å)	Lattice parameter (Å)			Lattice volume(Å ³)	$X_{c(XRD)}$ (%)
						a	b	c		
Virgin	(110)	18.74 ± 0.03	0.80 ± 0.01	99.03 ± 1.77	4.73 ± 0.01	7.83 ± 0.01	5.93 ± 0.01	10.29 ± 0.15	478.24 ± 8.39	29.28 ± 1.40
	(111)	20.65 ± 0.08	0.64 ± 0.01	124.85 ± 2.21	4.30 ± 0.02					
	(200)	22.68 ± 0.02	0.83 ± 0.07	97.49 ± 7.99	3.92 ± 0.01					
	(211)	28.78 ± 0.03	0.74 ± 0.06	110.16 ± 8.13	3.10 ± 0.01					
A2	(110)	18.76 ± 0.01	0.64 ± 0.03	124.59 ± 6.16	4.73 ± 0.01	7.83 ± 0.03	5.92 ± 0.01	10.11 ± 0.17	469.47 ± 8.80	28.28 ± 3.98
	(111)	20.73 ± 0.07	0.62 ± 0.01	128.87 ± 3.59	4.28 ± 0.02					
	(200)	22.68 ± 0.08	0.76 ± 0.03	105.81 ± 3.81	3.92 ± 0.02					
	(211)	28.85 ± 0.04	0.75 ± 0.03	108.29 ± 4.88	3.09 ± 0.01					
A4	(110)	18.76 ± 0.03	0.62 ± 0.03	128.14 ± 6.80	4.73 ± 0.01	7.82 ± 0.01	5.93 ± 0.01	10.11 ± 0.10	468.79 ± 3.70	25.10 ± 2.30
	(111)	20.73 ± 0.01	0.64 ± 0.02	124.41 ± 3.26	4.28 ± 0.01					
	(200)	22.74 ± 0.01	0.75 ± 0.02	106.82 ± 3.35	3.91 ± 0.01					
	(211)	28.80 ± 0.05	0.77 ± 0.01	105.82 ± 1.04	3.10 ± 0.01					
A8	(110)	18.76 ± 0.02	0.62 ± 0.01	128.36 ± 0.93	4.73 ± 0.01	7.81 ± 0.01	5.93 ± 0.01	9.90 ± 0.03	459.14 ± 1.60	24.26 ± 1.49
	(111)	20.81 ± 0.12	0.62 ± 0.02	128.09 ± 3.32	4.26 ± 0.01					
	(200)	22.74 ± 0.03	0.75 ± 0.01	106.47 ± 1.64	3.91 ± 0.01					
	(211)	28.83 ± 0.01	0.73 ± 0.02	110.87 ± 2.32	3.09 ± 0.01					
N2	(110)	18.73 ± 0.04	0.64 ± 0.01	124.41 ± 0.63	4.73 ± 0.01	7.84 ± 0.01	5.94 ± 0.02	9.98 ± 0.14	464.85 ± 6.33	27.56 ± 4.04
	(111)	20.75 ± 0.06	0.64 ± 0.01	124.66 ± 2.67	4.28 ± 0.02					
	(200)	22.66 ± 0.01	0.79 ± 0.02	101.65 ± 3.05	3.92 ± 0.01					
	(211)	28.80 ± 0.07	0.76 ± 0.01	106.38 ± 0.89	3.10 ± 0.01					
N4	(110)	18.79 ± 0.01	0.63 ± 0.01	125.74 ± 1.60	4.72 ± 0.01	7.81 ± 0.01	5.92 ± 0.01	10.04 ± 0.14	464.22 ± 5.83	27.47 ± 1.94
	(111)	20.78 ± 0.04	0.63 ± 0.03	126.53 ± 5.43	4.27 ± 0.01					
	(200)	22.76 ± 0.01	0.78 ± 0.01	103.38 ± 1.18	3.90 ± 0.01					
	(211)	28.80 ± 0.07	0.74 ± 0.01	109.44 ± 1.73	3.10 ± 0.01					
N8	(110)	18.77 ± 0.01	0.60 ± 0.02	132.59 ± 5.29	4.72 ± 0.01	7.80 ± 0.01	5.94 ± 0.01	9.98 ± 0.11	462.54 ± 5.10	25.17 ± 2.02
	(111)	20.78 ± 0.05	0.61 ± 0.02	131.98 ± 4.62	4.27 ± 0.01					
	(200)	22.77 ± 0.01	0.76 ± 0.04	107.82 ± 6.04	3.90 ± 0.01					
	(211)	28.83 ± 0.04	0.70 ± 0.04	115.88 ± 6.22	3.09 ± 0.01					
Ar2	(110)	18.76 ± 0.02	0.63 ± 0.01	125.43 ± 1.66	4.73 ± 0.01	7.81 ± 0.02	5.94 ± 0.01	10.04 ± 0.01	465.64 ± 1.91	28.22 ± 1.66
	(111)	20.76 ± 0.02	0.63 ± 0.01	127.00 ± 0.44	4.28 ± 0.01					
	(200)	22.75 ± 0.03	0.76 ± 0.03	105.23 ± 0.59	3.91 ± 0.01					
	(211)	28.82 ± 0.13	0.71 ± 0.01	113.59 ± 0.84	3.09 ± 0.01					
Ar4	(110)	18.73 ± 0.06	0.63 ± 0.01	127.12 ± 1.15	4.73 ± 0.01	7.81 ± 0.01	5.95 ± 0.02	10.00 ± 0.19	464.82 ± 6.28	28.11 ± 2.78
	(111)	20.75 ± 0.02	0.63 ± 0.01	126.05 ± 1.02	4.28 ± 0.01					
	(200)	22.75 ± 0.03	0.76 ± 0.01	105.03 ± 0.73	3.91 ± 0.01					
	(211)	28.82 ± 0.13	0.74 ± 0.01	110.05 ± 1.49	3.09 ± 0.01					
Ar8	(110)	18.76 ± 0.02	0.60 ± 0.02	133.33 ± 4.52	4.72 ± 0.01	7.80 ± 0.01	5.93 ± 0.01	10.00 ± 0.10	462.86 ± 4.01	25.66 ± 2.63
	(111)	20.79 ± 0.04	0.61 ± 0.02	131.40 ± 5.02	4.27 ± 0.01					
	(200)	22.77 ± 0.04	0.71 ± 0.03	112.74 ± 5.36	3.90 ± 0.01					
	(211)	28.77 ± 0.07	0.71 ± 0.04	114.13 ± 6.94	3.10 ± 0.01					

* 2θ is the diffraction angle, FWHM is the full width at half-maximum, d is the interplanar distance and $L_{(hkl)}$ is the apparent crystallite size in the direction perpendicular to (hkl) .

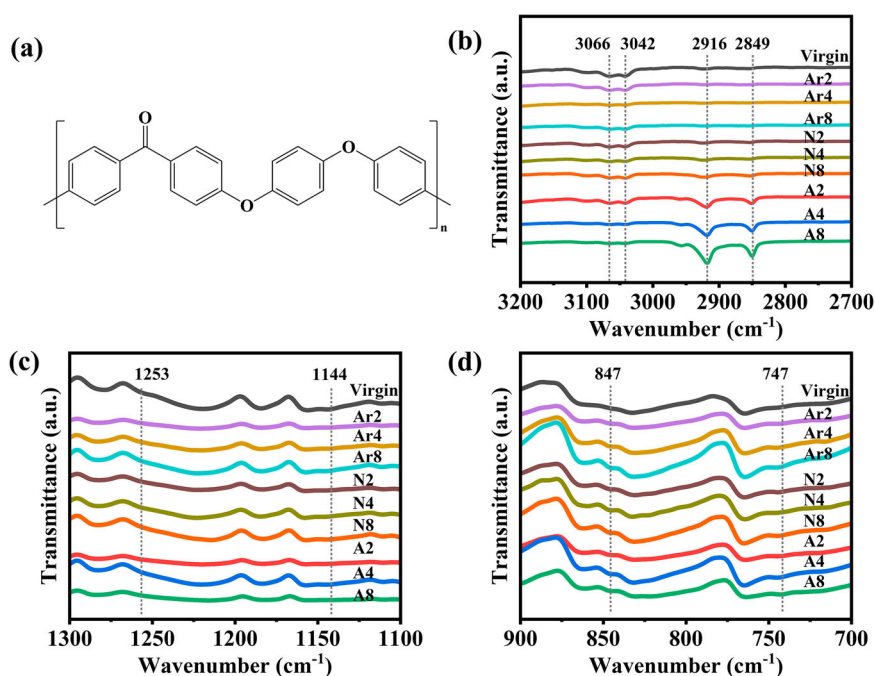


Figure 9. (a) Chemical repeat unit of the PEEK polymer and FTIR spectra of virgin and aged PEEK powders at wavenumbers of (b) 3200–2700, (c) 1300–1100, and (d) 900–700 cm^{-1} .

increased after thermal ageing, which is a result of the crosslinking of the macromolecular chains and subsequent formation of 1,2,4-trisubstituted benzene (Figure 9d) [32, 54]. Previous studies suggested that the absorption peaks at 1711, 1410, 1253, and 1147 cm^{-1} can be attributed to the degradation of PEEK molecular chains [23, 32, 53]. Negligible changes were found in the intensity and form of those signals after thermal ageing in argon and nitrogen, proving that both can be used as protective gases for SLS [55].

The FTIR spectra indicate that the PEEK powders did not degrade when maintained for a long time at the theoretical T_b under argon or nitrogen. The corresponding ageing mechanisms under different gases were as follows: chain crosslinking occurred inside the molecular chains of PEEK powder when thermally aged in air, nitrogen, or argon, whereas chain breakage was observed only when thermally aged in air (Figure 1b).

3.7. Reusability demonstration of aged PEEK powders for SLS

The virgin and thermally aged PEEK powders were sintered under the corresponding ageing gas condition, and the sintering parameters are reported in Section 2.2 and Table S1, supplementary material. First, single-layers of virgin PEEK powders could be successfully sintered at a laser power of 6 W, both in nitrogen and argon (Figure 10a and d). However, blackening and severe degradation were observed when sintered in air under

the same sintering parameters (Figure S5a, supplementary material). When lower powers were used to scan the platform, the powders failed to melt. A similar phenomenon was observed for A2, A4, and A8. As indicated in the FTIR results, the PEEK powders aged in air were partially decomposed, showing the highest degree of ageing in three gas conditions, which made them difficult to sinter when exposed to an oxygen-containing atmosphere at 330 °C; specifically, they were either severely decomposed at higher laser power or unmelted at lower laser power. This indicates that PEEK powders aged in air cannot be reused and emphasises the importance of using a protective gas in the high-temperature sintering of PEEK.

The DSC and XRD results showed that the crystallinity was gradually reduced in aged PEEK powders, for which less energy was required to fuse the powders. When scanned using a laser power of 6 W, samples fabricated by Ar2/N2, Ar4/N4, and Ar8/N8 (that is, under the protection of argon or nitrogen) were all blackened and degraded. The images shown in Figures S5b–d (supplementary material) are only for Ar2, Ar4, and Ar8 because the observations for N2, N4, and N8 were similar.

Attempts to avoid blackening and degradation involved gradually reducing the laser power; under these conditions, single-layer films of Ar2/N2, Ar4/N4, and Ar8/N8 (Figure 10g and j) could be sintered successfully at laser powers of 5.5, 5, and 4 W, respectively. Further, smooth surfaces were detected in the sintered

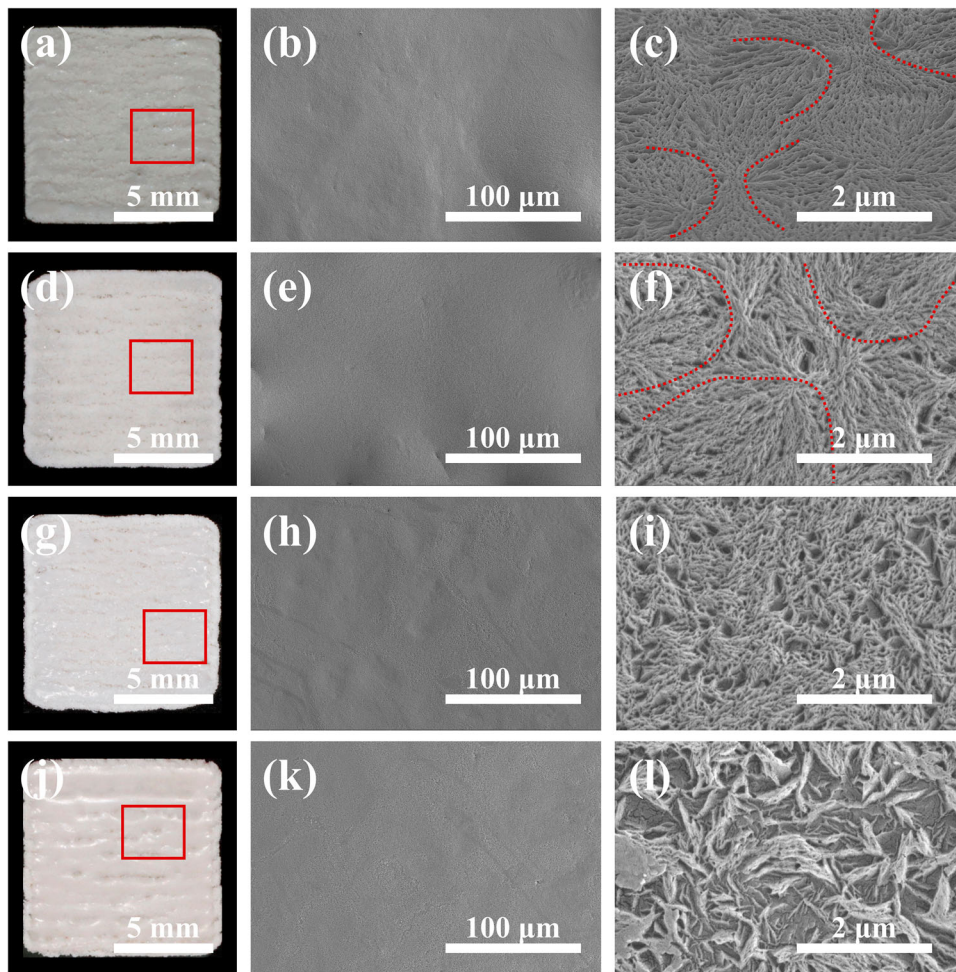


Figure 10. Single-layers and SEM images of virgin PEEK powders sintered in (a–c) argon and (d–f) nitrogen; (g–h) thermally aged Ar8 powders sintered in argon, and (i–l) thermally aged N8 powders sintered in nitrogen, respectively. Arcs indicate the crystal boundaries.

areas in both virgin and thermally aged samples (Figure 10b, e, h, k). However, at high magnifications, crystal boundaries were clearly observed in virgin PEEK printed samples (Figure 10c and f) but were not easy to detect in Ar8 and N8 (Figure 10i and l). In addition, the microdensities of Ar8 and N8 sintered samples were lower than that of virgin PEEK powder.

Microhardness testing is an easy, cheap, and non-destructive method for characterising the mechanical properties of small volumes of samples and has been used to study the performance of PEEK composites recently [56–58]. In this study, the Vickers hardness (HD) was used to evaluate the mechanical properties of the single layers of sintered virgin and aged PEEK powders prepared under different ageing conditions (Figure 11).

Compared with that of the virgin PEEK sintered in argon (Ar0), the HD of powders aged and sintered in argon was slightly reduced with the increasing of ageing time, but the changes were negligible. For example, even after 8 h ageing in argon, the HD of the

Ar8 sintered film was 14.11 ± 0.62 HV, which was 98% of that of Ar0 (14.39 ± 0.49 HV). The HD of virgin PEEK powder sintered in nitrogen (N0) was similar to that of Ar0, but those of N4 and N8 were reduced by 7.42%

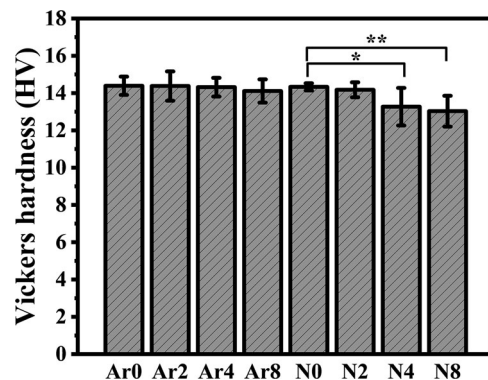


Figure 11. Vickers hardness of single-layer sintered samples from virgin and thermally aged PEEK powders. Ar0 refers to the virgin PEEK powders sintered in argon, and N0 refers to the virgin PEEK powders sintered in nitrogen.

Table 5. Recommendations for virgin and aged PEEK powder in the SLS process.

Sintering gas	Powder type	Sinterability (Yes/No)	SW (°C)	Laser power (W)
Argon	Virgin	Yes	303.57–332.07	6
	Ar2	Yes	307.62–332.64	5.5
	Ar4	Yes	308.36–332.64	5
	Ar8	Yes	311.09–332.29	4
Nitrogen	Virgin	Yes	303.57–332.07	6
	N2	Yes	305.91–332.64	5.5
	N4	Yes	306.59–332.63	5
	N8	Yes	311.09–333.32	4
Air	Virgin	No	303.57–332.07	/
	A2	No	311.83–333.32	/
	A4	No	313.54–333.09	/
	A8	No	313.89–332.64	/

and 9.10%, respectively, as a result of the relatively looser microstructure sintered in nitrogen (Figure 10). Although similar physico-chemical properties were observed for the PEEK powders aged in nitrogen or argon for the same holding time, the fabricated samples showed lower hardness for powders aged in nitrogen for more than 4 h, indicating that the degree of ageing in samples sintered in nitrogen was higher than that sintered in argon. This suggests that nitrogen may have negative effects on the sintering process, and argon is the preferred choice. The recommendations for using virgin and aged PEEK powder in the SLS process are presented in Table 5. In particular, the laser power should be reduced when reusing aged PEEK powders.

4. Conclusion

In this work, we systematically investigated the influence of ageing conditions on the changes in the physico-chemical properties of PEEK powders for SLS at the optimal powder bed temperature (330 °C) and have proposed guidelines for sintering parameters when reusing aged PEEK powders in the SLS process. The main conclusions are as follows:

- (1) Thermally aged PEEK powders exhibit narrower PSDs, improved flowability, enhanced bulk density, and more regular microstructures when aged in air, nitrogen, and argon.
- (2) Chain crosslinking occurred inside the molecular chains of PEEK powder when thermally aged in air, nitrogen, and argon, whereas chain breakage was found only when thermally aged in air. The crystallinity, lattice volume, and sintering window gradually decrease with the increase in holding time under the three gas conditions.
- (3) Stable hardness of single-layers sintered by reused PEEK was obtained in powders aged 8 h in argon,

and reduced hardness was obtained after ageing in nitrogen for 4 h. Argon is, thus, recommended as the protective gas both for virgin and aged PEEK powders in high-temperature SLS.

- (4) A reduced laser power should be used when reusing aged PEEK powders.

In summary, this study highlights the importance of using argon as the protective gas in the high-temperature SLS of PEEK and proves the potential for reusability of aged PEEK powders. Precise control of the powder bed temperature and reduced laser power is recommended when reusing aged PEEK powders. The assessment of multi-layers is the limitation in this work and will be investigated in future work.

Disclosure statement

No potential conflict of interest was reported by the author(s).

Funding

This work was supported by National Natural Science Foundation of China: [Grant Number No. 52035001]; Capital's Funds for Health Improvement and Research: [Grant Number No. 2022-2Z-4106].

ORCID

Yuqing Guo  <http://orcid.org/0000-0001-8299-6486>

Hu Chen  <http://orcid.org/0000-0001-6116-1279>

Sukun Tian  <http://orcid.org/0000-0001-8289-5968>

Yongxiang Xu  <http://orcid.org/0000-0002-3397-7809>

Kenan Ma  <http://orcid.org/0000-0003-1930-6184>

Shuai Ma  <http://orcid.org/0000-0002-6506-9506>

Xiang Wang  <http://orcid.org/0000-0002-9639-6040>

Yicha Zhang  <http://orcid.org/0000-0002-5219-1748>

Yuchun Sun  <http://orcid.org/0000-0002-3424-5028>

References

- [1] Wang H, Chen P, Wu H, et al. Comparative evaluation of printability and compression properties of poly-ether-ether-ketone triply periodic minimal surface scaffolds fabricated by laser powder bed fusion. *Addit Manuf.* 2022;57:102961. doi:10.1016/j.addma.2022.102961
- [2] Bai J, Yuan S, Shen F, et al. Toughening of polyamide 11 with carbon nanotubes for additive manufacturing. *Virtual Phys Prototyp.* 2017;12(3):235–240. doi:10.1080/17452759.2017.1315146
- [3] Sutton AT, Kriewall CS, Leu MC, et al. Powder characterization techniques and effects of powder characteristics on part properties in powder-bed fusion processes. *Virtual Phys Prototyp.* 2017;12(1):3–29. doi:10.1080/17452759.2016.1250605
- [4] Tiwari SK, Pande S, Agrawal S, et al. Selection of selective laser sintering materials for different applications. *Rapid*

- Prototyp J. 2015;21(6):630–648. doi:10.1108/rpj-03-2013-0027
- [5] Goh GL, Dikshit V, Koneru R, et al. Fabrication of design-optimized multifunctional safety cage with conformal circuits for drone using hybrid 3D printing technology. *Int J Adv Manuf Technol.* 2022;120:2573–2586. doi:10.1007/s00170-022-08831-y
- [6] Deckard CR. Method and apparatus for producing parts by selective sintering. US4863538. 1986.
- [7] Chavez LA, Ibañez P, Hassan MS, et al. Low-temperature selective laser sintering 3D printing of PEEK-nylon blends: impact of thermal post-processing on mechanical properties and thermal stability. *J Appl Polym Sci.* 2022: 52290. doi:10.1002/app.52290
- [8] Zarybnicka L, Petru J, Krpec P, et al. 2022. Effect of additives and print orientation on the properties of laser sintering-printed polyamide 12 components *Polymers (Basel)* 2022;14(6):1172. doi:10.3390/polym14061172
- [9] Kobayashi R, Yang M. Nondestructive observation of the surrounding powder in the vicinity of polymer laser-sintered specimens for understanding orange peel formation. *Rapid Prototyp J.* 2023;29(7):1395–1408. doi:10.1108/RPJ-08-2022-0268
- [10] Berretta S, Ghita O, Evans KE. Morphology of polymeric powders in laser sintering (LS): from polyamide to new PEEK powders. *Eur Polym J.* 2014;59:218–229. doi:10.1016/j.eurpolymj.2014.08.004
- [11] Wu T, Ren Y, Liang L, et al. Tensile strength and wear resistance of glass-reinforced PA1212 fabricated by selective laser sintering. *Virtual Phys Prototyp.* 2023;18(1): e2150652. doi:10.1080/17452759.2022.2150652
- [12] Wei Y, Xi S, Wang Z, et al. Improving selective laser sintering property of PA1212 powder by polydopamine: physical coating vs in-situ coating. *Powder Technol.* 2023;426:118605. doi:10.1016/j.powtec.2023.118605
- [13] Tonello R, Conradsen K, Pedersen DB, et al. Surface roughness and grain size variation when 3D printing polyamide 11 parts using selective laser sintering. *Polymers (Basel).* 2023;15:2967. doi:10.3390/polym15132967
- [14] Tian X, Peng G, Mengxue Y, et al. Process prediction of selective laser sintering based on heat transfer analysis for polyamide composite powders. *Int J Heat Mass Transfer.* 2018;120:379–386. doi:10.1016/j.ijheatmasstransfer.2017.12.045
- [15] Wang Y, Rouholamin D, Davies R, et al. Powder characteristics, microstructure and properties of graphite platelet reinforced poly ether ether ketone composites in high temperature laser sintering (HT-LS). *Mater Des.* 2015;88:1310–1320. doi:10.1016/j.matdes.2015.09.094
- [16] Berretta S, Evans KE, Ghita O. Processability of PEEK, a new polymer for high temperature laser sintering (HT-LS). *Eur Polym J.* 2015;68:243–266. doi:10.1016/j.eurpolymj.2015.04.003
- [17] Hoskins TJ, Dearn KD, Kukureka SN. Mechanical performance of PEEK produced by additive manufacturing. *Polym Test.* 2018;70:511–519. doi:10.1016/j.polymertesting.2018.08.008
- [18] Ghita OR, James E, Trimble R, et al. Physico-chemical behaviour of poly (ether ketone) (PEK) in high temperature laser sintering (HT-LS). *J Mater Process Technol.* 2014;214(4):969–978. doi:10.1016/j.jmatprotec.2013.11.007
- [19] Beard MA, Ghita OR, Bradbury J, et al. (2011). Material characterisation of additive manufacturing components made from a polyetherketone (PEK) high temperature thermoplastic polymer. Paper presented at the 5th International Conference on Advanced Research and Rapid Prototyping, Polytechn Inst Leiria, Sch Technol & Management, Leiria, PORTUGAL, Sep 28–Oct 01, 2011.
- [20] Chen P, Su J, Wang H, et al. Mechanical properties and microstructure characteristics of lattice-surfaced PEEK cage fabricated by high-temperature laser powder bed fusion. *J Mater Sci Technol.* 2022;125:105–117. doi:10.1016/j.jmst.2022.03.009
- [21] Yan M, Tian X, Peng G, et al. High temperature rheological behavior and sintering kinetics of CF/PEEK composites during selective laser sintering. *Compos Sci Technol.* 2018;165:140–147. doi:10.1016/j.compscitech.2018.06.023
- [22] Lai W, Wang Y, Fu H, et al. Hydroxyapatite/polyetheretherketone nanocomposites for selective laser sintering: thermal and mechanical performances. *E-Polymers.* 2020;20(1):542–549. doi:10.1515/epoly-2020-0057
- [23] Patel A, Venoor V, Yang F, et al. Evaluating poly(ether ether ketone) powder recyclability for selective laser sintering applications. *Polym Degrad Stab.* 2021;185:109502. doi:10.1016/j.polymdegradstab.2021.109502
- [24] Gomes PC, Pineiro OG, Alves AC, et al. On the reuse of SLS polyamide 12 powder. *Materials (Basel).* 2022;15(16):5486. doi:10.3390/ma15165486
- [25] Ghita O, James E, Davies R, et al. High temperature laser sintering (HT-LS): an investigation into mechanical properties and shrinkage characteristics of poly (ether ketone) (PEK) structures. *Mater Des.* 2014;61:124–132. doi:10.1016/j.matdes.2014.04.035
- [26] Berretta S, Evans KE, Ghita OR. Predicting processing parameters in high temperature laser sintering (HT-LS) from powder properties. *Mater Des.* 2016;105:301–314. doi:10.1016/j.matdes.2016.04.097
- [27] Benedetti L, Brule B, Decraemer N, et al. A route to improving elongation of high-temperature laser sintered PEKK. *Addit Manuf.* 2020;36:101540. doi:10.1016/j.addma.2020.101540
- [28] Chen P, Cai H, Li Z, et al. Crystallization kinetics of polyetheretherketone during high temperature-selective laser sintering. *Addit Manuf.* 2020;36:101615. doi:10.1016/j.addma.2020.101615
- [29] Hesse N, Winzer B, Peukert W, et al. Towards a generally applicable methodology for the characterization of particle properties relevant to processing in powder bed fusion of polymers – from single particle to bulk solid behavior *Addit Manuf.* 2021;41:101957. doi:10.1016/j.addma.2021.101957
- [30] Yi N, Davies R, Chaplin A, et al. Novel backbone modified polyetheretherketone (PEEK) grades for powder bed fusion with enhanced elongation at break. *Addit Manuf.* 2022;55:102857. doi:10.1016/j.addma.2022.102857
- [31] Yan M, Tian X, Yao R. Processability and reusability of CF/PEEK mixture for powder bed fusion of high strength composites. *Compos Commun.* 2022;35:101318. doi:10.1016/j.coco.2022.101318
- [32] Chen P, Su J, Wang H, et al. Aging mechanism of polyetheretherketone powder during layer-wise infrared radiation of high-temperature laser powder bed

- fusion. *Mater Des.* 2022;213:110348. doi:10.1016/j.matdes.2021.110348
- [33] Nazarov A, Skorniyakov I, Shishkovsky I. The setup design for selective laser sintering of high-temperature polymer materials with the alignment control system of layer deposition. *Machines.* 2018;6(1):11. doi:10.3390/machines6010011
- [34] ASTM International. (2000). ASTM C1444, Standard test method for measuring the angle of repose of free-flowing mold powders.
- [35] Standards Press of China. (2008). Methods of dust character test. GB/T 16913-2008.
- [36] Standards Press of China. (2004). Plastics–Differential scanning calorimetry (DSC)–Part 3: determination of temperature and enthalpy of melting and crystallization. GB/T 19466.3-2004.
- [37] Wang Y, Shen J, Yan M, et al. Poly ether ether ketone and its composite powder prepared by thermally induced phase separation for high temperature selective laser sintering. *Mater Des.* 2021;201:109510. doi:10.1016/j.matdes.2021.109510
- [38] Patterson AL. The Scherrer formula for X-ray particle size determination. *Phys Rev.* 1939;56(10):978–982. doi:10.1103/PhysRev.56.978
- [39] Sun H, Yang X, Wei K, et al. Non-isothermal crystallization kinetics of continuous glass fiber-reinforced poly(ether ether ketone) composites. *J Therm Anal Calorim.* 2019;138(1):369–378. doi:10.1007/s10973-019-08245-1
- [40] Ding R, Xu L, Li J, et al. Investigation and life expectancy prediction on poly(ether-ether-ketone) cables for thermo-oxidative aging in containment dome of nuclear power plant. *Polym Test.* 2021;103:107362. doi:10.1016/j.polymertesting.2021.107362
- [41] Li D, Xu S, Li J. Effect of thermal oxygen aging on the crystallization and insulation properties of polyether ether ketone. *J Appl Polym Sci.* 2023;140(16):e53745. doi:10.1002/app.53745
- [42] Yao YY, He WR, Li JX, et al. Thermal-radiation aging on oriented poly(ether-ether-ketone) sheets *J Nucl Mater.* 2022;570:153948. doi:10.1016/j.jnucmat.2022.153948
- [43] Rodzen K, Strachota A, Ribot F, et al. Reactivity of the tin homolog of POSS, butylstannoxane dodecamer, in oxygen-induced crosslinking reactions with an organic polymer matrix: study of long-time behavior *Polym Degrad Stab.* 2015;118:147–166. doi:10.1016/j.polymdegradstab.2015.04.020
- [44] Zhu C, Zhang H, Li J. Thermal aging study of PEEK for nuclear power plant containment dome. *J Polym Res.* 2022;29:5. doi:10.1007/s10965-021-02839-w
- [45] Knör N, Walter R, Hauptert F. Mechanical and thermal properties of nano-titanium dioxide-reinforced polyetheretherketone produced by optimized twin screw extrusion. *J Thermoplast Compos Mater.* 2011;24:185–205. doi:10.1177/0892705710369867
- [46] Peyre P, Rouchausse Y, Defauchy D, et al. Experimental and numerical analysis of the selective laser sintering (SLS) of PA12 and PEKK semi-crystalline polymers. *J Mater Process Technol.* 2015;225:326–336. doi:10.1016/j.jmatprotec.2015.04.030
- [47] Hay JN, Langford JI, Lloyd JR. Variation in unit cell parameters of aromatic polymers with crystallization temperature. *Polymer (Guildf).* 1989;30(3):489–493. doi:10.1016/0032-3861(89)90019-0
- [48] Wang P, Lin Q, Wang Y, et al. Comparative study of the crystallization behavior and morphologies of carbon and glass fiber reinforced poly(ether ether ketone) composites. *Polym Polym Compos.* 2021;29(8):1229–1239. doi:10.1177/0967391120965102
- [49] Doumeng M, Makhlof L, Berthet F, et al. A comparative study of the crystallinity of polyetheretherketone by using density, DSC, XRD, and Raman spectroscopy techniques. *Polym Test.* 2021;93:106878. doi:10.1016/j.polymertesting.2020.106878
- [50] Rodzen K, Sharma PK, McIlhagger A, et al. The direct 3D printing of functional PEEK/hydroxyapatite composites via a fused filament fabrication approach. *Polymers (Basel).* 2021;13(4):545. doi:10.3390/polym13040545
- [51] Reitman M, Jaekel D, Siskey R, et al. Chapter 4 – Morphology and crystalline architecture of polyaryletherketones. *PEEK Biomaterials Handbook.* 2nd Ed. 2019: 53–66. doi:10.1016/B978-0-12-812524-3.00004-1
- [52] Regis M, Bellare A, Pascolini T, et al. Characterization of thermally annealed PEEK and CFR-PEEK composites: structure-properties relationships. *Polym Degrad Stab.* 2017;136:121–130. doi:10.1016/j.polymdegradstab.2016.12.005
- [53] Gaitanelis D, Worrall C, Kazilas M. Detecting, characterising and assessing PEEK's and CF-PEEK's thermal degradation in rapid high-temperature processing. *Polym Degrad Stab.* 2022;204:110096. doi:10.1016/j.polymdegradstab.2022.110096
- [54] Eaborn C. The sadtler handbook of infrared spectra. *J Organomet Chem.* 1979;171(2):C44. doi:10.1016/S0022-328X(00)81552-1
- [55] Pascual A, Toma M, Tsotra P, et al. On the stability of PEEK for short processing cycles at high temperatures and oxygen-containing atmosphere. *Polym Degrad Stab.* 2019;165:161–169. doi:10.1016/j.polymdegradstab.2019.04.025
- [56] Goyal RK, Tiwari AN, Negi YS. Microhardness of PEEK/ceramic micro- and nanocomposites: correlation with Halpin-Tsai model. *Mater Sci amp; Eng A: Struct.* 2008;491(1-2):230–236. doi:10.1016/j.msea.2008.01.091
- [57] Kuo MC, Tsai CM, Huang JC, et al. PEEK composites reinforced by nano-sized SiO₂ and Al₂O₃ particulates. *Mater Chem Phys.* 2005;90(1):185–195. doi:10.1016/j.matchemphys.2004.10.009
- [58] Zhao T, Jiang Z, Ge Y, et al. Mechanical properties, biosafety, and shearing bonding strength of glass fiber-reinforced PEEK composites used as post-core materials. *J Mech Behav Biomed Mater.* 2023;145:106047. doi:10.1016/j.jmbbm.2023.106047